



Article

Conversion of Carbon Dioxide into Chemical Vapor Deposited Graphene with Controllable Number of Layers via Hydrogen Plasma Pre-Treatment

Yotsarayuth Seekaew^{1,2}, Nantikan Tammanoon¹, Adisorn Tuantranont¹, Tanom Lomas¹, Anurat Wisitsoraat^{1,*} and Chatchawal Wongchoosuk^{3,*}

¹ Graphene and Printed Electronics Research Division (GPERD), National Security and Dual-Use Technology Center, National Science and Technology Development Agency, 111 Thailand Science Park, Phahon Yothin Road, Klong Nueng, Klong Luang, Phatum Thani 12120, Thailand

² Department of Physics, Faculty of Science, Ramkhamhaeng University, Bang Kapi, Bangkok 10240, Thailand

³ Department of Physics, Faculty of Science, Kasetsart University, Chatuchak, Bangkok 10900, Thailand

* Correspondence: anurat.wisitsoraat@nectec.or.th (A.W.); chatchawal.w@ku.ac.th (C.W.)

Abstract: In this work, we report the conversion of carbon dioxide (CO₂) gas into graphene on copper foil by using a thermal chemical vapor deposition (CVD) method assisted by hydrogen (H₂) plasma pre-treatment. The synthesized graphene has been characterized by Raman spectroscopy, X-ray diffraction, scanning electron microscopy, and transmission electron microscopy. The results show the controllable number of layers (two to six layers) of high-quality graphene by adjusting H₂ plasma pre-treatment powers (100–400 W). The number of layers is reduced with increasing H₂ plasma pre-treatment powers due to the direct modification of metal catalyst surfaces. Bilayer graphene can be well grown with H₂ plasma pre-treatment powers of 400 W while few-layer graphene has been successfully formed under H₂ plasma pre-treatment powers ranging from 100 to 300 W. The formation mechanism is highlighted.

Keywords: graphene; carbon dioxide; hydrogen plasma; chemical vapor deposition



Citation: Seekaew, Y.; Tammanoon, N.; Tuantranont, A.; Lomas, T.; Wisitsoraat, A.; Wongchoosuk, C. Conversion of Carbon Dioxide into Chemical Vapor Deposited Graphene with Controllable Number of Layers via Hydrogen Plasma Pre-Treatment. *Membranes* **2022**, *12*, 796.

<https://doi.org/10.3390/membranes12080796>

Academic Editors: Konstantin Mikhelson, Beata Paczosa-Bator and Amir Razmjou

Received: 1 August 2022

Accepted: 16 August 2022

Published: 18 August 2022

Publisher's Note: MDPI stays neutral with regard to jurisdictional claims in published maps and institutional affiliations.



Copyright: © 2022 by the authors. Licensee MDPI, Basel, Switzerland. This article is an open access article distributed under the terms and conditions of the Creative Commons Attribution (CC BY) license (<https://creativecommons.org/licenses/by/4.0/>).

1. Introduction

Carbon dioxide (CO₂) is an important greenhouse gas in the atmosphere [1]. It helps to trap heat on our Earth's surface and supports the growth of plants in the agricultural cycle [2,3]. However, high emission of CO₂ produced by human activities, such as the combustion of fossil fuels to produce electricity, has recently caused serious problems in the form of global warming and climate change [4]. Moreover, exposure to atmospheric CO₂ at high levels produces a variety of human health effects [5]. To mitigate the adverse effects of high CO₂ emissions, there has been increasing research interest in CO₂ reduction and utilization [6–8]. One of the most compelling utilizations of CO₂ is to convert it into valuable products such as carbon-based nanomaterials, such as carbon quantum dots, inorganic nanoparticles, carbon nanotubes (CNTs) and graphene [9–14]. For examples, Kim et al. [15] synthesized the multi-walled CNTs by chemical vapor deposition (CVD) with NaBH₄ reductant and NiCl₂ catalyst. Ren et al. [16] demonstrated the preparation of carbon nanofibers via molten carbonate electrolysis from atmospheric CO₂. Molina-Jirón et al. [17] reported the growth of graphene via atmospheric-pressure CVD with a catalytic Cu-Pd alloy. Licht et al. [18] produced carbon nanofibers and CNTs from CO₂ using a solar thermal electrochemical process. Wang et al. [19] presented a transformation of CO₂ into a carbon nano-scaffold by using electrolysis in molten carbonate. Until now, the development of new methods or technologies for the conversion of CO₂ to valuable nanomaterials has been in great demand since CO₂ emission has become one of the biggest global concerns, and as net zero by 2050 is the goal.

Graphene is one of the well-known two-dimensional (2D) materials that has exceptional physical, chemical, and electrical properties [20–23]. Currently, graphene has been widely applied in several applications including nanoelectronics, flexible electronics, batteries, super-capacitors, solar cells, gas sensors, membranes, and chemical sensors [11,24–30]. Graphene can be grown by numerous methods including CVD, mechanical exfoliation, chemical oxidation/reduction and electrolytic exfoliation [31–33]. Among them, CVD is one of the most popular graphene growth methods because it can produce a high-quality monolayer and few-layer graphene [34–38]. The basic principle of thermal CVD relies on the decomposition of gas molecules, such as methane [39], acetylene [40], ethylene [36], and ethanol [41], to react with some metal catalysts and induce graphene growth. Without metal catalysts on substrates, a high temperature of up to 1650 °C is required to overcome the large energy barrier for graphene nucleation [42].

In this work, we report the conversion of CO₂ into graphene on copper foil substrates using a CVD method with hydrogen (H₂) plasma pre-treatment. To our best knowledge, this is the first work to investigate the effects of H₂ plasma pre-treatment to convert CO₂ into graphene with the controllable few layers. Our finding demonstrates the important role of H₂ plasma pre-treatment in the formation of few-layer graphene (two–six layers) by adjusting radio frequency (rf) powers for plasma pre-treatments (100–400 W).

2. Materials and Methods

Copper (Cu) foil (25 µm thick, 99.98% metals basis) was purchased from Sigma-Aldrich Co., LLC, Darmstadt, Germany. The graphene was grown on the Cu foil by CVD method using CO₂ gas (99.999% purity) as a carbon source, as shown in Figure 1. The growth process was conducted using a customized thermal CVD system integrated with an inductively coupled plasma system (planarGROW-4S, planarTECH LLC, The Woodlands, TX, USA). The distance from the plasma coil to the sample was ~75 cm. Before the Cu foil was loaded into a 4" horizontal quartz tube of the CVD system, it was washed in ethanol solution for 10 min under ultrasonication and dried in air at room temperature. After the loading of samples, 150 sccm of H₂ flowed into the CVD quartz tube while the reactor was heated to 1000 °C at a pressure of 1 Torr. At 1000 °C, the Cu foil surface was treated using H₂ plasma generated by rf power for 30 min. The rf power was adjusted from 100 to 400 W in order to investigate the effects of H₂ plasma pre-treatment. Next, a mixture of CO₂ (50 sccm) and H₂ (200 sccm) was applied at a working pressure of 2 Torr for 30 min for graphene growth on Cu foils. After the graphene growth stage, the CVD quartz tube reactor was cooled down to room temperature under an H₂ flow of 150 sccm at 1 Torr. In the CVD process, the heating rate was set at 15 °C/min while the cooling rate was set at 10 °C/min. The graphene samples were characterized by field-emission scanning electron microscopy (FE-SEM: SU8030, Hitachi, Tokyo, Japan), X-ray diffraction (XRD: D8 Advance, Bruker, MA, USA), transmission electron microscopy (TEM: JEM-2100 Plus, JEOL, Tokyo, Japan), and Raman spectroscopy (InVia Raman Microscope, Renishaw, West Dundee, IL, USA) using a laser with an excitation wavelength of 785 nm.

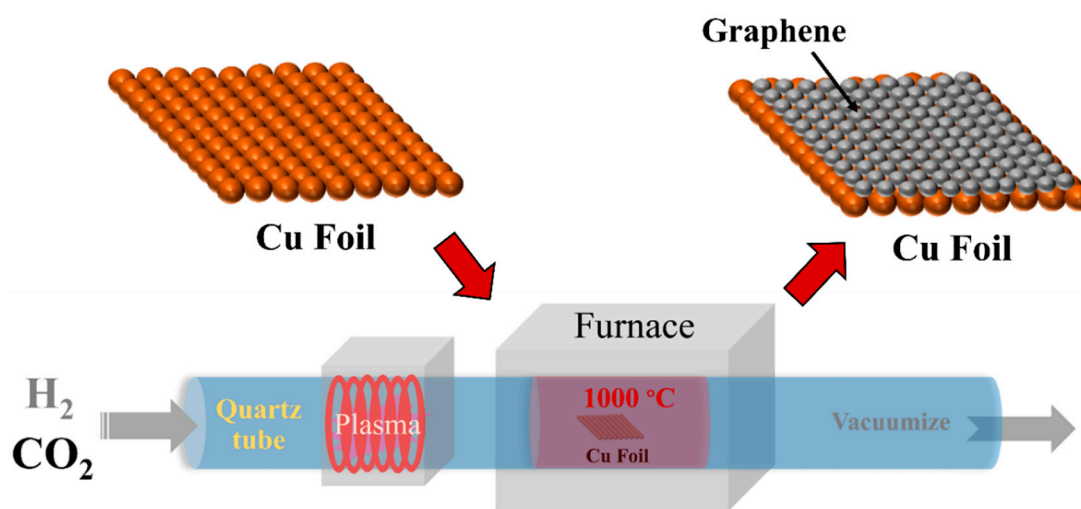


Figure 1. Schematic diagram for the conversion of CO₂ to graphene on a Cu foil by the chemical vapor deposition (CVD) method.

3. Results and Discussion

After the growth process, all samples were initially characterized by Raman spectroscopy as presented in Figure 2. It is evident that only the samples with H₂ plasma pre-treatment (rf power = 100–400 W) exhibit D, G and 2D peaks at around 1300, 1580 and 2600 cm⁻¹, respectively (Figure 2a). It is well known that the D peak is associated with lattice defects of the graphene structure while the G peak corresponds to primary sp²-hybridized carbon bonds in graphene. The 2D peak is the second order of the D band relating to one boundary defect in graphene [43,44]. Therefore, they confirm the formation of graphene on Cu surfaces with H₂ plasma pre-treatments. At the same growth condition, no graphene was observed on Cu surfaces without H₂ plasma pre-treatment. This indicates that the H₂ plasma pre-treatment plays an important role in modifying the Cu surface for graphene nucleation.

To investigate the quality and number of graphene layers, the intensity ratios of the 2D to G band (I_{2D}/I_G) and D to G band (I_D/I_G) were calculated from the Raman spectra and are displayed in Figure 2b. The I_{2D}/I_G is known to be strongly related to the number of layers [34,45–47]. The $I_{2D}/I_G > 2$ indicates the monolayer graphene while $1 < I_{2D}/I_G < 2$ and $I_{2D}/I_G < 1$ refer to the bilayer and trilayer/few-layer graphene, respectively. In Figure 2b, the I_{2D}/I_G increases from 0.47 to 1.06 with increasing rf plasma power from 100 W to 400 W, suggesting the formation of few-layer graphene and the decrease of the number of graphene layers to two on increasing the H₂ plasma rf power to 400 W. Concerning the graphene quality, the I_D/I_G decreases from 2.33 to 0.37 as the rf plasma power increases from 100 W to 400 W. The decrease of the I_D/I_G intensity ratio implies the reduction of defect density. At the high plasma powers of 300–400 W, the I_D/I_G intensity ratio is as low as ~0.37, indicating graphene structures with low defect levels [48].

The graphene growth evolution with respect to the growth times, including 15, 30 and 45 min, using the rf plasma power of 400 W, is shown in Figure 3. At all reaction times, the grown surfaces exhibit three main Raman peaks (D, G and 2D), indicating that graphene has already formed at 15 min, with $I_{2D}/I_G \sim 1$ corresponding to the bilayer graphene structure. However, I_D/I_G (0.80) at 15 min is relatively high compared with I_D/I_G at 30 min (0.37) because the nucleated graphene is initially defective and these defects may be amended with additionally deposited atoms as the time progresses. For the extended growth time of 45 min, more layers of graphene are formed, leading to a significantly reduced I_{2D}/I_G in accordance with the previous reports of other CVD graphene growth studies using different times [49–51].

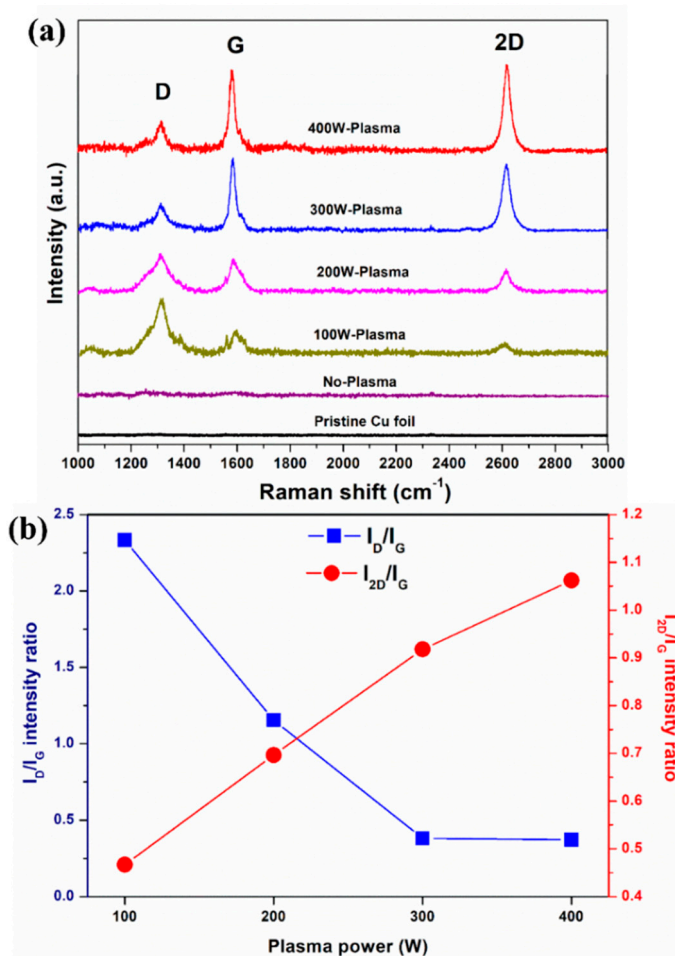


Figure 2. Raman spectra of (a) graphene growth on Cu foils pre-treated with different H₂ rf plasma powers and (b) their intensity ratio values of I_D/I_G and I_{2D}/I_G. It should be noted that the H₂ gas still flowed over the sample with the rf power off in the case of “No-Plasma”.

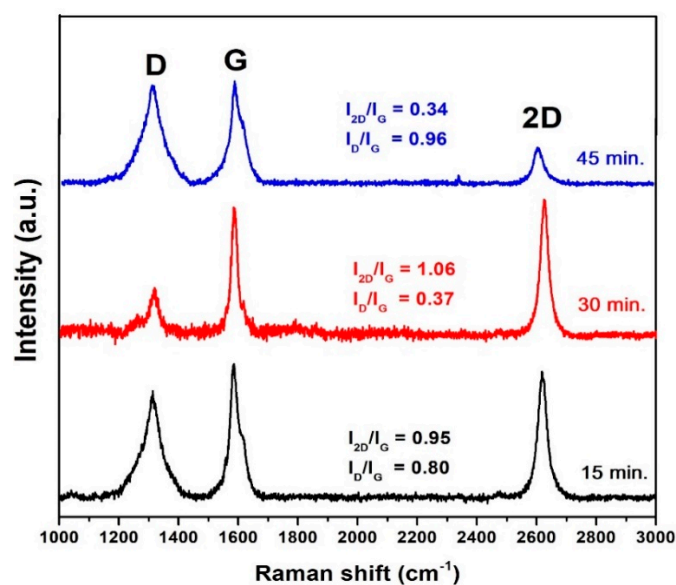


Figure 3. Raman spectra of graphene growth on Cu foils pre-treated with H₂ rf plasma power of 400 W at different growth times.

To evaluate the effects of H₂ rf plasma power during pre-treatment on graphene growth, the XRD patterns of the pristine Cu foil and the graphene growth on Cu foils pre-treated with different H₂ rf plasma powers are displayed in Figure 4. As seen in Figure 4a, all samples exhibit three pronounced peaks located at 43.34°, 50.46° and 74.16°, corresponding to Cu (111), Cu (200) and Cu (220) (JCPDS No. 65-9026), respectively [52,53]. Interestingly, Cu₂O (111) phase at 37° [54,55] arises in comparison with pristine Cu (unheated) and samples with H₂ plasma pre-treatments after the sample was heated to the growth temperature (1000 °C) in the CVD system (Figure 4b). The formation of Cu₂O during the CVD process can suppress the graphene's growth. With H₂ plasma pre-treatments, Cu₂O is absent and the C (002) peak at ~26° is detected, dictating the formation of graphene on Cu foil without other defect peaks in accordance with the Raman results, which indicate high quality graphene structures.

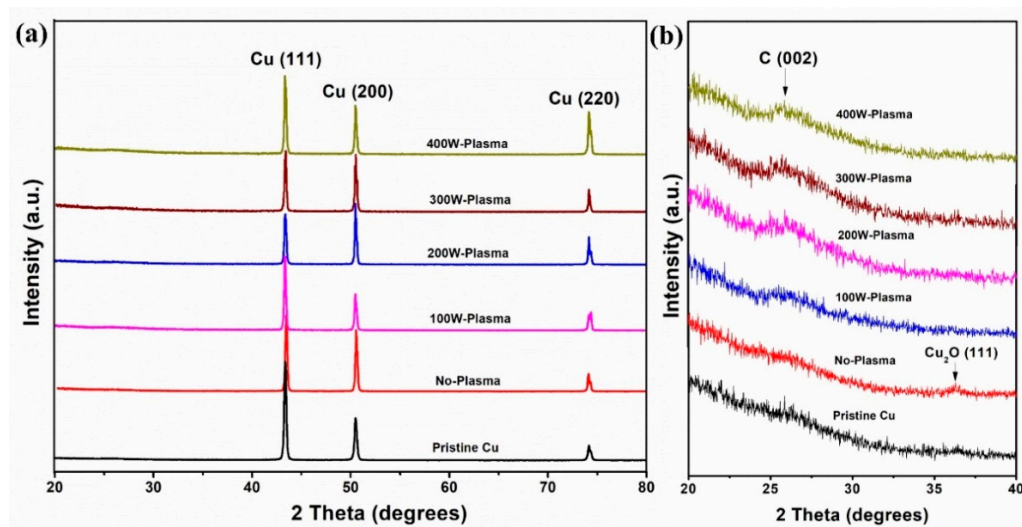


Figure 4. (a) XRD patterns and (b) zoom graph of XRD patterns of the pristine Cu and the graphene growth on Cu foils pre-treated with different H₂ rf plasma powers.

The detailed surface morphologies of graphene grown from CO₂ on Cu foils pre-treated with varying H₂ rf plasma powers are demonstrated in Figure 5. It clearly shows that the H₂ plasma pre-treatment strongly affects the surface morphology of Cu foil. In this work, Cu foil acts as both catalyst and substrate. During the high-temperature CVD process, the recrystallization of Cu grain occurs and Cu₂O is formed on the surface due to oxidation by residual oxygen. With H₂ plasma pre-treatment, high rf powers can contribute to the removal of residual copper oxides on the surface as shown in Figure 5c–f. An increase of the rf plasma power results in a remarkable reduction in the density of residual oxides and enhances the carbon in-diffusion-controlled kinetics of CO₂ flow in the reactor, leading to the formation of graphene. However, a large number of wrinkles are formed and some secondary nucleation always dominates. The wrinkles are caused by the discontinuous growth of monolayer graphene associated with the difference in thermal expansion between graphene and Cu [56,57]. Thus, only bilayer and few-layer graphene can be formed. In addition, the wrinkles of graphene on the Cu substrate are quite similar to the few-layer graphene wrinkles formed on other substrates such as Ni foam [58].

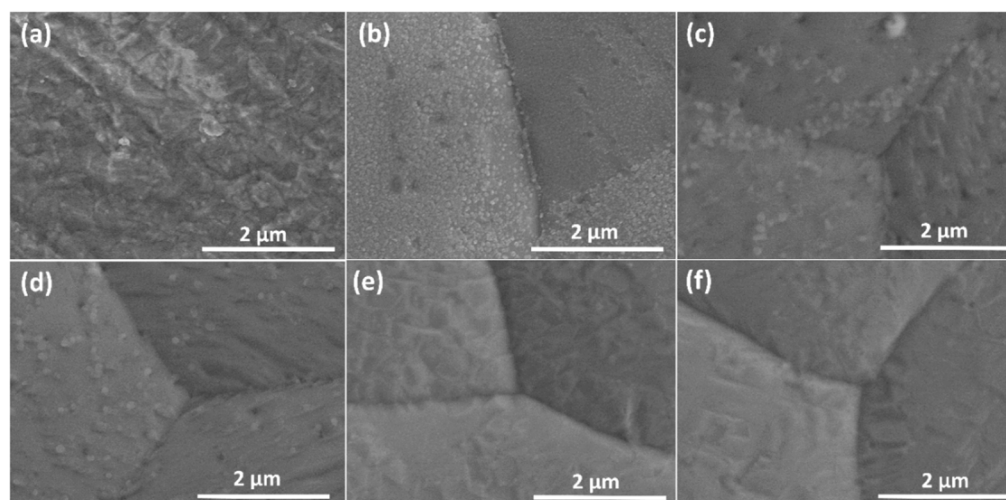


Figure 5. FE-SEM images of (a) pristine Cu foil, Cu foil after CVD growth with (b) no and with hydrogen plasma pre-treatment using rf powers of (c) 100 W, (d) 200 W, (e) 300 W and (f) 400 W for 30 min.

The number of layers of graphene grown on Cu foils pre-treated with different plasma powers was verified by high-resolution (HR) TEM images as displayed in Figure 6. The HR-TEM images clearly show graphene fringes displaying bilayer, trilayers, four layers, and six layers in accordance with the Raman results of graphene grown on Cu foils pre-treated with the plasma powers of 400, 300, 200 and 100 W, respectively. The thickness of graphene with bilayer, trilayers, four layers, and six layers is estimated to be ~ 0.69 nm, 1.18 nm, 1.64 nm and 2.50 nm, respectively. In addition, the interlayer spacing of graphene sheets can be determined to be ~ 0.35 nm in agreement with many other publications [17,59,60]. The selected area electron diffraction (SAED) pattern, as illustrated in the inset of Figure 6a, presents two sets of six-fold reflection spots of a hexagonal lattice. This evidence confirms the bilayer graphene structure with high quality [61].

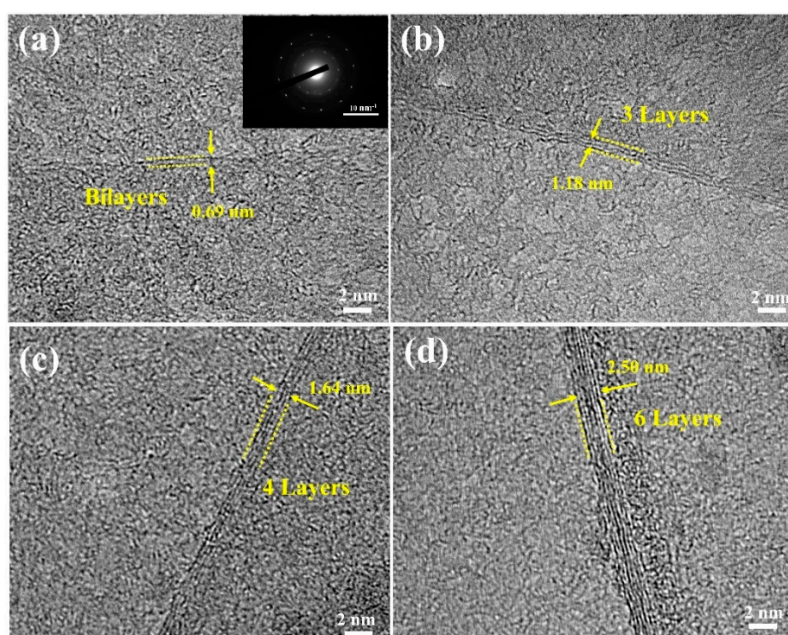


Figure 6. Representative high-resolution TEM images of graphene edges produced via hydrogen plasma pre-treatments with rf powers of (a) 400 W, (b) 300 W, (c) 200 W, and (d) 100 W. The inset shows a typical SAED pattern of the bilayer graphene.

The sheet resistances as a function of the rf plasma powers were also investigated as shown in Figure 7. The sheet resistance of graphene increases from ~75 to 100 Ω/sq on increasing the rf plasma power from 100 to 400 W. The number of graphene layers strongly correlates to band structure, energy gap, Fermi energy, and charge carriers, which directly affect the electrical conductivity [34,62–64]. From the characterization results, the number of graphene layers was six at 100 W and was reduced to two at 400 W. Both bilayer and multilayer graphene structures exhibit typical parabolic band structures associated with finite effective masses and charge carriers, which decrease with a decreasing number of graphene layers [34]. Bilayer graphene has more available electronic states in its valence band, leading to higher sheet resistances compared with multilayer graphene. In comparison with other substrates, the sheet resistance of graphene grown on Cu foil is smaller than that on PMMA and glass substrates (540–650 Ω/sq of bilayer and 300–350 Ω/sq of trilayer) [65,66]. The obtained low sheet resistance may be attributed to the uniformity of graphene film on the Cu surface and low defects compared with those produced by other methods [67]. To confirm the uniformity of graphene over the sample surface, FE-SEM images of bilayer graphene at five different regions on the Cu foil are displayed in Figure 8. It demonstrates that all regions show similar surface and wrinkle features of bilayer graphene on the Cu foil. Thus, the obtained bilayer graphene is highly uniform over the sample area.

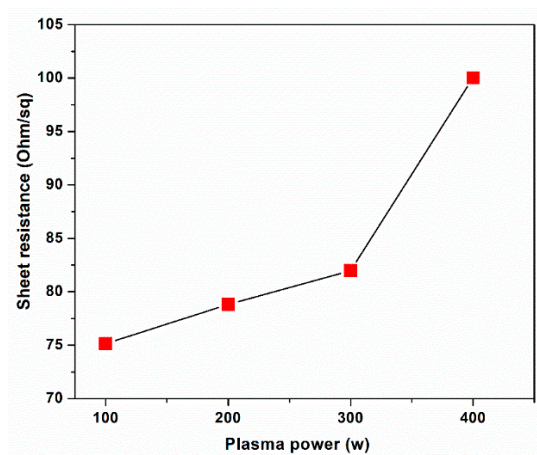


Figure 7. Sheet resistance of graphene on Cu foil as a function of the H₂ plasma power.

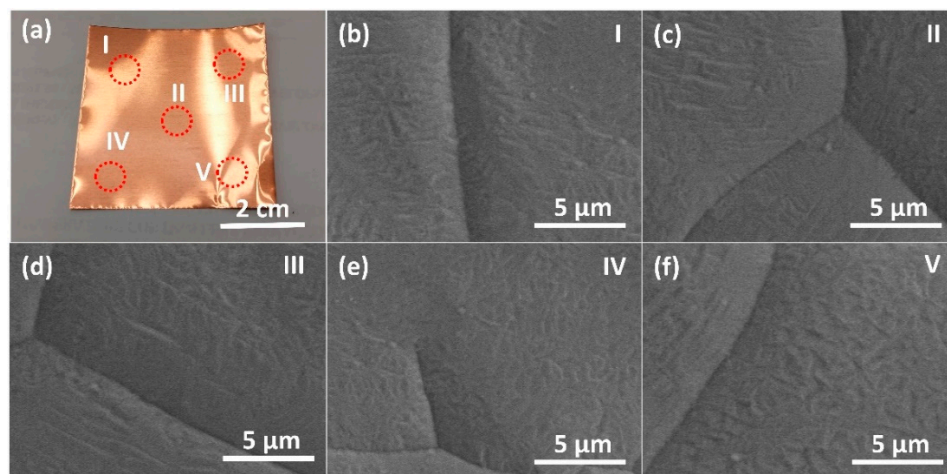


Figure 8. (a) Photograph of the real sample (Cu foil) after graphene growth with H₂ plasma pre-treatment at 400 W for 30 min. (b–f) FE-SEM images of bilayer graphene at five different regions on the Cu foil.

The growth mechanism of CVD graphene depends on many factors, such as hydrocarbon gas source, pressure, flow rate, temperature, growth time, catalyst and substrate [68]. Several catalysts, such as Ni/Al₂O₃ [69], Cu-Pd [17], and NaCl–CaCl₂–CaO [70], have been used to activate CO₂ for the graphene growth. In this work, Cu foils act as both catalyst and substrate while only H₂ plasma pre-treatment is used to activate the Cu catalyst with fixed temperature and time. Based on the characterization results, the H₂ plasma power strongly affects the metal catalyst surface properties. Therefore, the formation of graphene with different numbers of layers is attributed to distinct metal catalyst surfaces pre-treated with different H₂ plasma powers. In the synthesis step, CO₂ is introduced as a carbon source for graphene growth. At high temperatures (~1000 °C), CO₂ begins to decompose into carbon and oxygen atoms, generating CO and O [71], while CO₂ can also directly react with H₂ leading to the formation of H₂O or other molecules (methane and methanol) [72,73]. The reaction for converting CO₂ to graphene on the Cu surface can be described as $\text{CO}_2 + 2\text{H}_2 \rightarrow \text{C} + 2\text{H}_2\text{O}$ [17]. However, copper oxide (Cu₂O) formed on metal surfaces at high temperatures can suppress the diffusion of carbon species on the metal catalyst's surface, preventing the nucleation of graphene. According to a previous study, graphene nucleation densities are low when Cu surfaces are relatively rough compared with the atomic thinness of the graphene [74]. From the results in this work, graphene cannot be formed without H₂ plasma pre-treatment. The application of the H₂ plasma pre-treatment on Cu foil can reduce residues on the surface and make the surface smoother. By increasing the H₂ plasma power, residues are additionally removed, leading to an increasingly smooth Cu surface. The ingrained surface impurities act as nucleation sites for carbon adsorption during growth. Additional nucleation sites may be activated by H₂ plasma pre-treatment to form the multilayer graphene. The H₂ plasma power during pre-treatment can be thus used as a primary factor to control the number layers of graphene. In other words, C atoms dissociated from CO₂ at a high growth temperature can diffuse the Cu surface into bulk to start the nucleation and growth of graphene on the catalyst's surface. If the Cu surface confronts a contamination (oxidation of the unwanted impurities) before the precursor exposure, supersaturation of the surface is readily reached, limiting the nucleation of graphene. The H₂ plasma pre-treatment can remove the contaminations on the catalyst surface and activate Cu active sites for graphene growth.

4. Conclusions

In conclusion, CO₂ gas has successfully been converted into graphene films on Cu foils by way of a CVD method with H₂ plasma pre-treatment. Raman spectroscopy, XRD, SEM, and TEM data demonstrate the formation of high-quality graphene with two–six layers on Cu foils. Without H₂ plasma pre-treatment, a rough Cu surface with the cluster of oxide residues formed at a high growth temperature can suppress the diffusion of carbon species, resulting in no graphene nucleation. The introduction of the H₂ plasma pre-treatment can remove residuals and enhance the CO₂ flow kinetics on the Cu surface, assisting the nucleation and growth of graphene. The number of layers of graphene can be well controlled by varying the H₂ plasma powers applied for the direct modification of metal catalyst surfaces before graphene growth. The proposed method requires no additional carrier gas and a catalyst for graphene growth from CO₂. Therefore, it can be useful as an alternative way to convert CO₂ greenhouse gas in the atmosphere into a valuable graphene film with a controllable number of layers.

Author Contributions: Conceptualization, Y.S. and A.W.; methodology, Y.S., N.T. and A.W.; validation, C.W.; formal analysis, Y.S., A.W. and C.W.; investigation, Y.S. and A.W.; resources A.T., T.L. and A.W.; data curation, Y.S. and N.T.; writing—original draft preparation, Y.S.; writing—review and editing, C.W. and A.W.; visualization, Y.S.; supervision, A.T., T.L. and A.W., funding acquisition, Y.S., A.W. and C.W. All authors have read and agreed to the published version of the manuscript.

Funding: This work was financially supported by Program Management Unit for National Competitiveness Enhancement (PMU-C), National Research Council of Thailand (N41A640126) and Kasetsart University Research and Development Institute (FF(KU) 25.64).

Institutional Review Board Statement: Not applicable.

Informed Consent Statement: Not applicable.

Data Availability Statement: The data presented in this study are available on request from the corresponding author.

Acknowledgments: The authors gratefully acknowledged the research funding in the project entitled, Synthesis of Graphene from Carbon Dioxide Waste for Industrial Applications (P2051414), from Program Management Unit for National Competitiveness Enhancement (PMU-C) and the Thailand Research Fund for TRF Research Team Promotion Grant (RTA6180004). The Research Grant for Talented Young Researchers (N41A640126) from National Research Council of Thailand (NRCT), Post-doctoral Fellowship Program from National Science and Technology Development Agency (NSTDA) and Kasetsart University Research and Development Institute (FF(KU) 25.64) are acknowledged.

Conflicts of Interest: The authors declare no conflict of interest.

References

1. Chen, J.; Xing, Y.; Wang, Y.; Zhang, W.; Guo, Z.; Su, W. Application of iron and steel slags in mitigating greenhouse gas emissions: A review. *Sci. Total Environ.* **2022**, *844*, 157041. [[CrossRef](#)] [[PubMed](#)]
2. Cheng, W.; Duan, X.; Moore, J.C.; Deng, X.; Luo, Y.; Huang, L.; Wang, Y. Unevenly distributed CO₂ and its impacts on surface energy balance. *Atmos. Res.* **2022**, *274*, 106196. [[CrossRef](#)]
3. Seesaard, T.; Goel, N.; Kumar, M.; Wongchoosuk, C. Advances in gas sensors and electronic nose technologies for agricultural cycle applications. *Comput. Electron. Agric.* **2022**, *193*, 106673. [[CrossRef](#)]
4. Carnicer, J.; Alegria, A.; Giannakopoulos, C.; Di Giuseppe, F.; Karali, A.; Koutsias, N.; Lionello, P.; Parrington, M.; Vitolo, C. Global warming is shifting the relationships between fire weather and realized fire-induced CO₂ emissions in Europe. *Sci. Rep.* **2022**, *12*, 10365. [[CrossRef](#)]
5. Jacobson, T.A.; Kler, J.S.; Hernke, M.T.; Braun, R.; Meyer, K.C.; Funk, W.E. Direct human health risks of increased atmospheric carbon dioxide. *Nat. Sustain.* **2019**, *2*, 691–701. [[CrossRef](#)]
6. Chen, J.; Abazari, R.; Adegoke, K.A.; Maxakato, N.W.; Bello, O.S.; Tahir, M.; Tasleem, S.; Sanati, S.; Kirillov, A.M.; Zhou, Y. Metal–organic frameworks and derived materials as photocatalysts for water splitting and carbon dioxide reduction. *Coord. Chem. Rev.* **2022**, *469*, 214664. [[CrossRef](#)]
7. Xie, W.-H.; Li, H.; Yang, M.; He, L.-N.; Li, H.-R. CO₂ capture and utilization with solid waste. *Green Chem. Eng.* **2022**, *3*, 199–209. [[CrossRef](#)]
8. Arayawut, O.; Kerdcharoen, T.; Wongchoosuk, C. Structures, Electronic Properties, and Gas Permeability of 3D Pillared Silicon Carbide Nanostructures. *Nanomaterials* **2022**, *12*, 1869. [[CrossRef](#)]
9. Wickramasinghe, S.; Wang, J.; Morsi, B.; Li, B. Carbon Dioxide Conversion to Nanomaterials: Methods, Applications, and Challenges. *Energy Fuels* **2021**, *35*, 11820–11834. [[CrossRef](#)]
10. Kondee, S.; Arayawut, O.; Pon-On, W.; Wongchoosuk, C. Nitrogen-doped carbon oxide quantum dots for flexible humidity sensor: Experimental and SCC-DFTB study. *Vacuum* **2022**, *195*, 110648. [[CrossRef](#)]
11. Chaloeipote, G.; Samarnwong, J.; Traiwatcharanon, P.; Kerdcharoen, T.; Wongchoosuk, C. High-performance resistive humidity sensor based on Ag nanoparticles decorated with graphene quantum dots. *R. Soc. Open Sci.* **2021**, *8*, 210407. [[CrossRef](#)] [[PubMed](#)]
12. Traiwatcharanon, P.; Siriwatcharapiboon, W.; Jongprateep, O.; Wongchoosuk, C. Electrochemical paraquat sensor based on lead oxide nanoparticles. *RSC Adv.* **2022**, *12*, 16079–16092. [[CrossRef](#)] [[PubMed](#)]
13. Kerdcharoen, T.; Wongchoosuk, C. Carbon nanotube and metal oxide hybrid materials for gas sensing. In *Semiconductor Gas Sensors*; Woodhead Publishing Series in Electronic and Optical Materials; Jaaniso, R., Tan, O.K., Eds.; Woodhead Publishing: Cambridge, UK, 2013; pp. 386–407. [[CrossRef](#)]
14. Saengsonachai, A.; Seekaew, Y.; Traiwatcharanon, P.; Wongchoosuk, C. Dual functions of alternating current electroluminescent device for light emission and humidity detection. *Nanotechnology* **2022**, *33*, 405202. [[CrossRef](#)] [[PubMed](#)]
15. Kim, G.M.; Lim, W.-G.; Kang, D.; Park, J.H.; Lee, H.; Lee, J.; Lee, J.W. Transformation of carbon dioxide into carbon nanotubes for enhanced ion transport and energy storage. *Nanoscale* **2020**, *12*, 7822–7833. [[CrossRef](#)] [[PubMed](#)]
16. Ren, J.; Li, F.F.; Lau, J.; Urbina, L.G.; Licht, S. One-pot synthesis of carbon nanofibers from CO₂. *Nano Lett.* **2015**, *15*, 6142–6148. [[CrossRef](#)]
17. Molina-Jirón, C.; Chellali, M.R.; Kumar, C.N.S.; Kübel, C.; Velasco, L.; Hahn, H.; Moreno-Pineda, E.; Ruben, M. Direct conversion of CO₂ to multi-layer graphene using Cu-Pd alloys. *ChemSusChem* **2019**, *12*, 3509–3514. [[CrossRef](#)]
18. Licht, S.; Douglas, A.; Ren, J.; Carter, R.; Lefler, M.; Pint, C.L. Carbon Nanotubes Produced from Ambient Carbon Dioxide for Environmentally Sustainable Lithium-Ion and Sodium-Ion Battery Anodes. *ACS Cent. Sci.* **2016**, *2*, 162–168. [[CrossRef](#)]

19. Wang, X.; Licht, G.; Liu, X.; Licht, S. One pot facile transformation of CO₂ to an unusual 3-D nano-scaffold morphology of carbon. *Sci. Rep.* **2020**, *10*, 21518. [[CrossRef](#)]
20. Razaq, A.; Bibi, F.; Zheng, X.; Papadakis, R.; Jafri, S.H.M.; Li, H. Review on Graphene-, Graphene Oxide-, Reduced Graphene Oxide-Based Flexible Composites: From Fabrication to Applications. *Materials* **2022**, *15*, 1012. [[CrossRef](#)]
21. Seekaew, Y.; Arayawut, O.; Timsorn, K.; Wongchoosuk, C. Chapter Nine—Synthesis, characterization, and applications of graphene and derivatives. In *Carbon-Based Nanofillers and Their Rubber Nanocomposites*; Yaragalla, S., Mishra, R., Thomas, S., Kalarikkal, N., Maria, H.J., Eds.; Elsevier: Amsterdam, The Netherlands, 2019; pp. 259–283. [[CrossRef](#)]
22. Mazlan, N.A.; Butt, F.S.; Lewis, A.; Yang, Y.; Yang, S.; Huang, Y. The Growth of Metal–Organic Frameworks in the Presence of Graphene Oxide: A Mini Review. *Membranes* **2022**, *12*, 501. [[CrossRef](#)]
23. Ghuge, A.D.; Shirode, A.R.; Kadam, V.J. Graphene: A Comprehensive Review. *Curr. Drug Targets* **2017**, *18*, 724–733. [[CrossRef](#)] [[PubMed](#)]
24. Seesaard, T.; Wongchoosuk, C. Recent Progress in Electronic Noses for Fermented Foods and Beverages Applications. *Fermentation* **2022**, *8*, 302. [[CrossRef](#)]
25. Zare, P.; Aleemardani, M.; Seifalian, A.; Bagher, Z.; Seifalian, A. Graphene Oxide: Opportunities and Challenges in Biomedicine. *Nanomaterials* **2021**, *11*, 1083. [[CrossRef](#)] [[PubMed](#)]
26. Permatasari, F.A.; Irham, M.A.; Bisri, S.Z.; Iskandar, F. Carbon-Based Quantum Dots for Supercapacitors: Recent Advances and Future Challenges. *Nanomaterials* **2021**, *11*, 91. [[CrossRef](#)]
27. Goldoni, R.; Farronato, M.; Connelly, S.T.; Tartaglia, G.M.; Yeo, W.-H. Recent advances in graphene-based nanobiosensors for salivary biomarker detection. *Biosens. Bioelectron.* **2021**, *171*, 112723. [[CrossRef](#)]
28. Traiwatcharanon, P.; Siriwatcharapiboon, W.; Wongchoosuk, C. Electrochemical Sodium Ion Sensor Based on Silver Nanoparticles/Graphene Oxide Nanocomposite for Food Application. *Chemosensors* **2020**, *8*, 58. [[CrossRef](#)]
29. Olabi, A.G.; Abdelkareem, M.A.; Wilberforce, T.; Sayed, E.T. Application of graphene in energy storage device—A review. *Renew. Sustain. Energy Rev.* **2021**, *135*, 110026. [[CrossRef](#)]
30. Arunragsa, S.; Seekaew, Y.; Pon-On, W.; Wongchoosuk, C. Hydroxyl edge-functionalized graphene quantum dots for gas-sensing applications. *Diam. Relat. Mater.* **2020**, *105*, 107790. [[CrossRef](#)]
31. Banerjee, A.N. Green syntheses of graphene and its applications in internet of things (IoT)—A status review. *Nanotechnology* **2022**, *33*, 322003. [[CrossRef](#)]
32. Kumar, N.; Salehiyan, R.; Chauke, V.; Bothoko, O.J.; Setshedi, K.; Scriba, M.; Masukume, M.; Ray, S.S. Top-down synthesis of graphene: A comprehensive review. *FlatChem* **2021**, *27*, 100224. [[CrossRef](#)]
33. Stankovich, S.; Dikin, D.A.; Piner, R.D.; Kohlhaas, K.A.; Kleinhammes, A.; Jia, Y.; Wu, Y.; Nguyen, S.T.; Ruoff, R.S. Synthesis of graphene-based nanosheets via chemical reduction of exfoliated graphite oxide. *Carbon* **2007**, *45*, 1558–1565. [[CrossRef](#)]
34. Seekaew, Y.; Phokharatkul, D.; Wisitsoraat, A.; Wongchoosuk, C. Highly sensitive and selective room-temperature NO₂ gas sensor based on bilayer transferred chemical vapor deposited graphene. *Appl. Surf. Sci.* **2017**, *404*, 357–363. [[CrossRef](#)]
35. Shen, C.; Yan, X.; Qing, F.; Niu, X.; Stehle, R.; Mao, S.S.; Zhang, W.; Li, X. Criteria for the growth of large-area adlayer-free monolayer graphene films by chemical vapor deposition. *J. Mater.* **2019**, *5*, 463–470. [[CrossRef](#)]
36. Trinsoutrot, P.; Vergnes, H.; Causat, B. Three dimensional graphene synthesis on nickel foam by chemical vapor deposition from ethylene. *Mater. Sci. Eng. B* **2014**, *179*, 12–16. [[CrossRef](#)]
37. Lee, K.; Lee, J.; Kwon, K.W.; Park, M.-S.; Hwang, J.-H.; Kim, K.J. 3D graphene-Ni foams an advanced electrode for high-performance nonaqueous redox flow batteries. *ACS Appl. Mater. Interfaces* **2017**, *9*, 22502–22508. [[CrossRef](#)]
38. Chen, Z.; Ren, W.; Gao, L.; Liu, B.; Pei, S.; Cheng, H.-M. Three-dimensional flexible and conductive interconnected graphene networks grown by chemical vapour deposition. *Nat. Mater.* **2011**, *10*, 424–428. [[CrossRef](#)]
39. Strudwick, A.J.; Weber, N.E.; Schwab, M.G.; Kettner, M.; Weitz, R.T.; Wunsch, J.R.; Müllen, K.; Sachdev, H. Chemical Vapor Deposition of High Quality Graphene Films from Carbon Dioxide Atmospheres. *ACS Nano* **2015**, *9*, 31–42. [[CrossRef](#)]
40. Xiao, T.; Hu, X.; Heng, B.; Chen, X.; Huang, W.; Tao, W.; Wang, H.; Tang, Y.; Tan, X.; Huang, X. Ni(OH)₂ nanosheets grown on graphene-coated nickel foam for high-performance pseudocapacitors. *J. Alloys Compd.* **2013**, *549*, 147–151. [[CrossRef](#)]
41. Jiang, F.; Fang, Y.; Xue, Q.; Chen, L.; Lu, Y. Graphene-based carbon nano-fibers grown on thin-sheet sinter-locked Ni-fiber as self-supported electrodes for supercapacitors. *Mater. Lett.* **2010**, *64*, 199–202. [[CrossRef](#)]
42. Zheng, S.; Zhong, G.; Wu, X.; D’Arsiè, L.; Robertson, J. Metal-catalyst-free growth of graphene on insulating substrates by ammonia-assisted microwave plasma-enhanced chemical vapor deposition. *RSC Adv.* **2017**, *7*, 33185–33193. [[CrossRef](#)]
43. Wang, P.; Zhang, D.; Zhang, L.; Fang, Y. The SERS study of graphene deposited by gold nanoparticles with 785 nm excitation. *Chem. Phys. Lett.* **2013**, *556*, 146–150. [[CrossRef](#)]
44. Klar, P.; Lidorikis, E.; Eckmann, A.; Verzhbitskiy, I.; Ferrari, A.C.; Casiraghi, C. Raman scattering efficiency of graphene. *Phys. Rev. B* **2013**, *87*, 205435. [[CrossRef](#)]
45. Tu, Z.; Liu, Z.; Li, Y.; Yang, F.; Zhang, L.; Zhao, Z.; Xu, C.; Wu, S.I.; Liu, H.; Yang, H.; et al. Controllable growth of 1–7 layers of graphene by chemical vapor deposition. *Carbon* **2014**, *73*, 252–258. [[CrossRef](#)]
46. Ni, Z.H.; Wang, H.M.; Kasim, J.; Fan, H.M.; Yu, T.; Wu, Y.H.; Feng, Y.P.; Shen, Z.X. Graphene Thickness Determination Using Reflection and Contrast Spectroscopy. *Nano Lett.* **2007**, *7*, 2758–2763. [[CrossRef](#)]
47. Fang, L.; Yuan, W.; Wang, B.; Xiong, Y. Growth of graphene on Cu foils by microwave plasma chemical vapor deposition: The effect of in-situ hydrogen plasma post-treatment. *Appl. Surf. Sci.* **2016**, *383*, 28–32. [[CrossRef](#)]

48. Kim, K.S.; Zhao, Y.; Jang, H.; Lee, S.Y.; Kim, J.M.; Kim, K.S.; Ahn, J.-H.; Kim, P.; Choi, J.-Y.; Hong, B.H. Large-scale pattern growth of graphene films for stretchable transparent electrodes. *Nature* **2009**, *457*, 706–710. [[CrossRef](#)]
49. Jin, Y.; Hu, B.; Wei, Z.; Luo, Z.; Wei, D.; Xi, Y.; Zhang, Y.; Liu, Y. Roles of H₂ in annealing and growth times of graphene CVD synthesis over copper foil. *J. Mater. Chem. A* **2014**, *2*, 16208–16216. [[CrossRef](#)]
50. Regmi, M.; Chisholm, M.F.; Eres, G. The effect of growth parameters on the intrinsic properties of large-area single layer graphene grown by chemical vapor deposition on Cu. *Carbon* **2012**, *50*, 134–141. [[CrossRef](#)]
51. Son, I.H.; Song, H.J.; Kwon, S.; Bachmatiuk, A.; Lee, S.J.; Benayad, A.; Park, J.H.; Choi, J.-Y.; Chang, H.; Rummeli, M.H. CO₂ enhanced chemical vapor deposition growth of few-layer graphene over NiOx. *ACS Nano* **2014**, *8*, 9224–9232. [[CrossRef](#)]
52. Zhang, Q.; Qin, Z.; Luo, Q.; Wu, Z.; Liu, L.; Shen, B.; Hu, W. Microstructure and nanoindentation behavior of Cu composites reinforced with graphene nanoplatelets by electroless co-deposition technique. *Sci. Rep.* **2017**, *7*, 1338. [[CrossRef](#)]
53. Zhang, Q.; Luo, Q.; Qin, Z.; Liu, L.; Wu, Z.; Shen, B.; Hu, W. Self-Assembly of Graphene-Encapsulated Cu Composites for Nonenzymatic Glucose Sensing. *ACS Omega* **2018**, *3*, 3420–3428. [[CrossRef](#)] [[PubMed](#)]
54. Jang, L.-W.; Zhang, L.; Menghini, M.; Cho, H.; Hwang, J.Y.; Son, D.I.; Locquet, J.-P.; Seo, J.W. Multilayered graphene grafted copper wires. *Carbon* **2018**, *139*, 666–671. [[CrossRef](#)]
55. Kim, D.; Resasco, J.; Yu, Y.; Asiri, A.M.; Yang, P. Synergistic geometric and electronic effects for electrochemical reduction of carbon dioxide using gold–copper bimetallic nanoparticles. *Nat. Commun.* **2014**, *5*, 4948. [[CrossRef](#)]
56. Yang, F.; Liu, Y.; Wu, W.; Chen, W.; Gao, L.; Sun, J. A facile method to observe graphene growth on copper foil. *Nanotechnology* **2012**, *23*, 475705. [[CrossRef](#)] [[PubMed](#)]
57. Zhang, Y.H.; Wang, B.; Zhang, H.R.; Chen, Z.Y.; Zhng, Y.; Sui, Y.P.; Li, X.L.; Xie, X.M.; Yu, G.H.; Jin, Z.; et al. The distribution of wrinkles and their effects on the oxidation resistance of chemical vapor deposition graphene. *Carbon* **2014**, *70*, 81–86. [[CrossRef](#)]
58. Seekaew, Y.; Wongchoosuk, C. A novel graphene-based electroluminescent gas sensor for carbon dioxide detection. *Appl. Surf. Sci.* **2019**, *479*, 525–531. [[CrossRef](#)]
59. Nakamura, M.; Kawai, T.; Irie, M.; Yuge, R.; Iijima, S.; Bandow, S.; Yudasaka, M. Graphite-like thin sheets with even-numbered layers. *Carbon* **2013**, *61*, 644–647. [[CrossRef](#)]
60. Yan, Y.; Manickam, S.; Lester, E.; Wu, T.; Pang, C.H. Synthesis of graphene oxide and graphene quantum dots from miscanthus via ultrasound-assisted mechano-chemical cracking method. *Ultrason. Sonochem.* **2021**, *73*, 105519. [[CrossRef](#)]
61. Hernandez-Robles, A.; Romeu, D.; Ponce, A. On the Mechanism Controlling the Relative Orientation of Graphene Bi-Layers. *Symmetry* **2022**, *14*, 719. [[CrossRef](#)]
62. Amer, M.S.; Mohammed, M.K.; Al Mafrage, A.M. Graphene to graphite; a layer by layer experimental measurements and density function theory calculations of electric conductivity. *Philos. Mag.* **2020**, *100*, 2491–2502. [[CrossRef](#)]
63. Fang, X.-Y.; Yu, X.-X.; Zheng, H.-M.; Jin, H.-B.; Wang, L.; Cao, M.-S. Temperature- and thickness-dependent electrical conductivity of few-layer graphene and graphene nanosheets. *Phys. Lett. A* **2015**, *379*, 2245–2251. [[CrossRef](#)]
64. Cho, J.H.; Na, S.R.; Park, S.; Akinwande, D.; Liechti, K.M.; Cullinan, M.A. Controlling the number of layers in graphene using the growth pressure. *Nanotechnology* **2019**, *30*, 235602. [[CrossRef](#)] [[PubMed](#)]
65. Suk, J.W.; Kitt, A.; Magnuson, C.W.; Hao, Y.; Ahmed, S.; An, J.; Swan, A.K.; Goldberg, B.B.; Ruoff, R.S. Transfer of CVD-Grown Monolayer Graphene onto Arbitrary Substrates. *ACS Nano* **2011**, *5*, 6916–6924. [[CrossRef](#)] [[PubMed](#)]
66. Wu, W.; Yu, Q.; Peng, P.; Liu, Z.; Bao, J.; Pei, S.-S. Control of thickness uniformity and grain size in graphene films for transparent conductive electrodes. *Nanotechnology* **2012**, *23*, 035603. [[CrossRef](#)] [[PubMed](#)]
67. Kato, R.; Tsugawa, K.; Okigawa, Y.; Ishihara, M.; Yamada, T.; Hasegawa, M. Bilayer graphene synthesis by plasma treatment of copper foils without using a carbon-containing gas. *Carbon* **2014**, *77*, 823–828. [[CrossRef](#)]
68. Saeed, M.; Alshammari, Y.; Majeed, S.A.; Al-Nasrallah, E. Chemical vapor deposition of graphene-synthesis, characterisation, and applications: A Review. *Molecules* **2020**, *25*, 3856. [[CrossRef](#)]
69. Luo, B.; Liu, H.; Jiang, L.; Jiang, L.; Geng, D.; Wu, B.; Hu, W.; Liu, Y.; Yu, G. Synthesis and morphology transformation of single-crystal graphene domains based on activated carbon dioxide by chemical vapor deposition. *J. Mater. Chem. C* **2013**, *1*, 2990–2995. [[CrossRef](#)]
70. Hu, L.; Song, Y.; Jiao, S.; Liu, Y.; Ge, J.; Jiao, H.; Zhu, J.; Wang, J.; Zhu, H.; Fray, D.J. Direct Conversion of Greenhouse Gas CO₂ into Graphene via Molten Salts Electrolysis. *ChemSusChem* **2016**, *9*, 588–594. [[CrossRef](#)]
71. Svavil’Nyi, M.Y.; Panarin, V.Y.; Shkola, A.A.; Nikolenko, A.S.; Strelchuk, V.V. Plasma Enhanced Chemical Vapor Deposition synthesis of graphene-like structures from plasma state of CO₂ gas. *Carbon* **2020**, *167*, 132–139. [[CrossRef](#)]
72. Lu, L.; Sun, X.; Ma, J.; Yang, D.; Wu, H.; Zhang, B.; Zhang, J.; Han, B. Highly Efficient Electroreduction of CO₂ to Methanol on Palladium-Copper Bimetallic Aerogels. *Angew. Chem. Int. Ed.* **2018**, *57*, 14149–14153. [[CrossRef](#)]
73. Vaiano, V.; Sannino, D.; Ciambelli, P. Steam reduction of CO₂ on Pd/TiO₂ catalysts: A comparison between thermal and photocatalytic reactions. *Photochem. Photobiol. Sci.* **2015**, *14*, 550–555. [[CrossRef](#)] [[PubMed](#)]
74. Braeuninger-Weimer, P.; Brennan, B.; Pollard, A.J.; Hofmann, S. Understanding and Controlling Cu-Catalyzed Graphene Nucleation: The Role of Impurities, Roughness, and Oxygen Scavenging. *Chem. Mater.* **2016**, *28*, 8905–8915. [[CrossRef](#)] [[PubMed](#)]